nature chemistry

ARTICLES

https://doi.org/10.1038/s41557-022-01018-8

Check for updates

Polyoxometalates as ligands to synthesize, isolate and characterize compounds of rare isotopes on the microgram scale

Ian Colliard[1,2], Jonathan R. I. Lee[3], Christopher A. Colla[4], Harris E. Mason[5,6], April M. Sawvel[3], Mavrik Zavarin[1], May Nyman[2] and Gauthier J.-P. Deblonde[1,5]✉

The synthesis and study of radioactive compounds are both inherently limited by their toxicity, cost and isotope scarcity. Traditional methods using small inorganic or organic complexes typically require milligrams of sample—per attempt—which for some isotopes is equivalent to the world's annual supply. Here we demonstrate that polyoxometalates (POMs) enable the facile formation, crystallization, handling and detailed characterization of metal–ligand complexes from microgram quantities owing to their high molecular weight and controllable solubility properties. Three curium–POM complexes were prepared, using just 1–10 μg per synthesis of the rare isotope $^{248}Cm^{3+}$, and characterized by single-crystal X-ray diffraction, showing an eight-coordinated Cm^{3+} centre. Moreover, spectrophotometric, fluorescence, NMR and Raman analyses of several *f*-block element–POM complexes, including $^{243}Am^{3+}$ and $^{248}Cm^{3+}$, showed otherwise unnoticeable differences between their solution versus solid-state chemistry, and actinide versus lanthanide behaviour. This POM-driven strategy represents a viable path to isolate even rarer complexes, notably with actinium or transcalifornium elements.

The synthesis and characterization of metal–ligand complexes provide invaluable information on the coordination chemistry and physicochemical properties of elements across the periodic table. However, such studies are particularly challenging for radioelements due to the inherent radiological hazard and limited access to compatible research facilities. A lesser-known aspect of radiochemistry is the high cost and low isotope availability, which severely restrict the experimental space and chemical systems investigated. This situation is particularly taxing to the development of actinide chemistry. Actinide research isotopes are only produced by a handful of institutions worldwide and only in minute quantities: milligram scale for americium, curium, berkelium and californium, tens of micrograms for actinium, a few micrograms for einsteinium and less for heavier elements[1]. This situation slows progress in our understanding of this part of the periodic table inasmuch as the amount of information available on each element is directly correlated to its isotopes' scarcity, cost and our ability to characterize small samples. For instance, ~80 years after Seaborg introduced the actinide concept[2,3], only ~600 Np complexes have been reported in the crystallographic databases[4–6], ~300 for Pu, <50 for Am, <10 for Cm, Bk and Cf, and none for Ac or the transcalifornium elements. For comparison, >17,000 uranium compounds have been characterized by single-crystal X-ray diffraction (SCXRD), and >100,000 for abundant metals such as iron, zinc or cobalt.

Furthermore, most structural data on transplutonium coordination compounds have only been obtained within the past decade, notably with the first Bk complexes characterized by SCXRD in 2016 (Bk^{3+}–dipicolinate and Bk^{3+}–borate) by Albrecht-Schmitt and co-workers[7], followed by three more in 2017–2019[8,9]. A handful of Cf or Cm compounds have also been structurally characterized very recently (Supplementary Table 1), culminating with the Cm^{3+}–mellitate, Cm^{3+}–pyrrolidinedithiocarbamate and Cf^{3+}–bis-metallocene-chloride complexes in 2020 and 2021[10,11]. While these recent breakthroughs have proven invaluable to the advancement of the *f*-element sciences, the synthesis of each complex required milligram quantities, hence dramatically increasing the cost and radiological constraints, and severely limiting the number of compounds investigated. These synthetic procedures are also inapplicable to even rarer materials such as actinium[12–14] and transcalifornium[15–18] complexes, which have thus only been probed by spectroscopy, solution thermodynamics or computation.

Previous studies focused on small inorganic or organic ligands (<1,000 g mol^{-1}). However, using small ligands further limits the study of radiometals because their complexes have a high content of the studied isotopes (Fig. 1a), leading to high material consumption and self-radiolysis issues[18]. In our search for an alternative strategy, we posited that using heavier ligands could alleviate this conundrum. Lacunary polyoxometalates (POMs) appeared ideally suited, being versatile high-molecular-weight ligands (2,000–20,000 g mol^{-1}) consisting of certain *d*-block metals, oxygen atoms and heteroatoms (for example, P, B, S, Se, Te, Si, Ge, As and Sb) that can complex a central metal ion (Fig. 1b). POMs represent the heaviest and densest class of ligands that can be characterized by high-resolution spectroscopies, including small-molecule SCXRD, contrary to other heavy ligands such as metalloproteins[19–23]. Moreover, POMs are radiation-resistant (a key feature in the study of radioisotopes), they crystallize relatively easily, and their structural and spectroscopic properties are driven by the metal centre. Despite their optimum

[1]Glenn T. Seaborg Institute, Physical and Life Sciences Directorate, Lawrence Livermore National Laboratory, Livermore, CA, USA. [2]Department of Chemistry, Oregon State University, Corvallis, OR, USA. [3]Material Sciences Division, Lawrence Livermore National Laboratory, Livermore, CA, USA. [4]Atmospheric, Earth and Energy Division, Lawrence Livermore National Laboratory, Livermore, CA, USA. [5]Nuclear and Chemical Sciences Division, Lawrence Livermore National Laboratory, Livermore, CA, USA. [6]Present address: Chemistry Division, Los Alamos National Laboratory, Los Alamos, NM, USA. ✉e-mail: Deblonde1@LLNL.gov

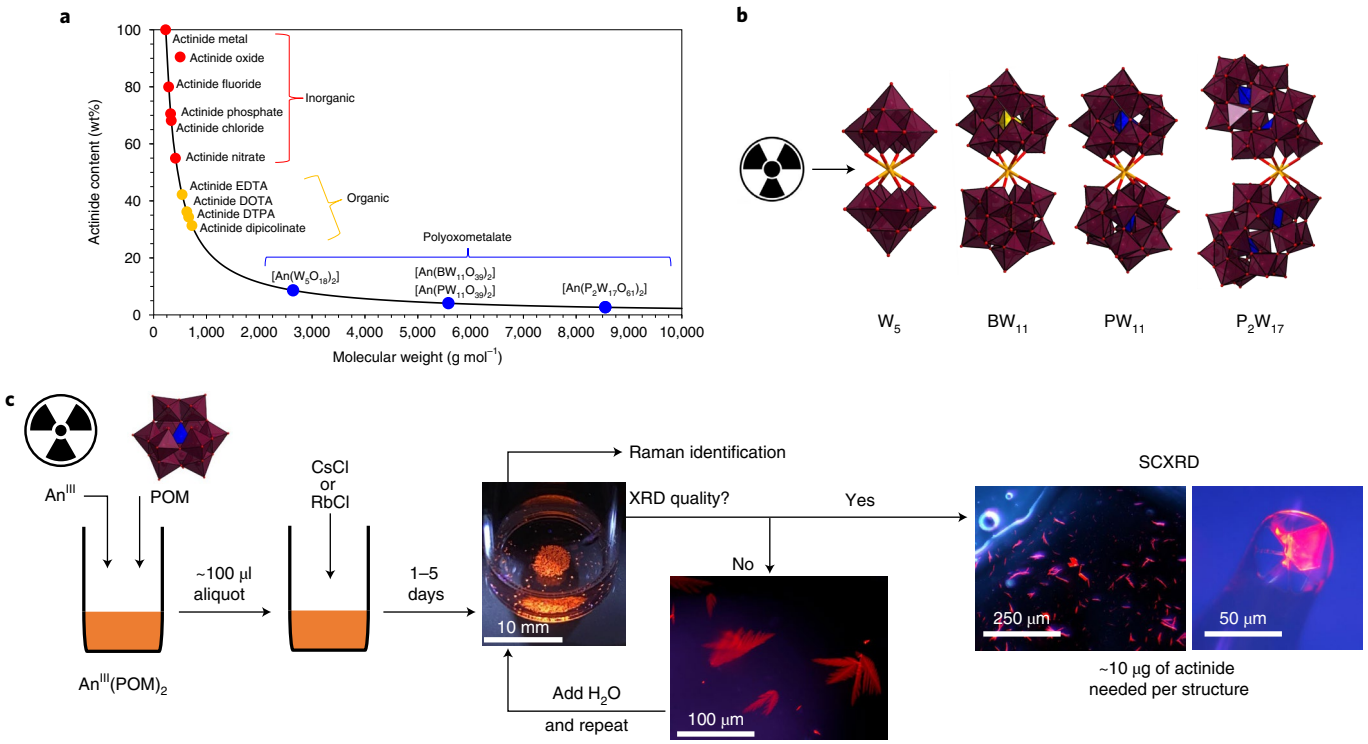

Fig. 1 | Leveraging POMs to obtain detailed structural information on actinide complexes from microgram quantities. a, Comparison of POMs with typical ligands studied with actinides. POM complexes contain minimal amounts of the difficult-to-study isotopes, such as actinide (An), while rendering high-resolution tools applicable (for example, SCXRD and Raman microscopy). The molecular weights were calculated using ^{248}Cm, as a representative actinide, but the proposed strategy remains valid for other isotopes (for example, ^{227}Ac, ^{244}Pu, $^{243/241}$Am, ^{249}Bk, ^{249}Cf and ^{254}Es). Counter ions have been omitted for simplification. The molecular weight of the POM compounds can be further increased by using heavy counter ions (for example, Rb^+, Cs^+ and tetrabutylammonium). **b**, Structures of the actinide–POM complexes investigated in the present work, namely $[An^{III}(W_5O_{18})_2]^{9-}$, $[An^{III}(BW_{11}O_{39})_2]^{15-}$, $[An^{III}(PW_{11}O_{39})_2]^{11-}$ and $[An^{III}(P_2W_{17}O_{61})_2]^{17-}$ (An = Am^{3+}, Cm^{3+}). W_5, $W_5O_{18}^{6-}$; BW_{11}, $BW_{11}O_{39}^{9-}$; PW_{11}, $PW_{11}O_{39}^{7-}$; P_2W_{17}, $P_2W_{17}O_{61}^{10-}$. Colour code: orange, An; maroon, W; blue, P; yellow, B; red, O. See Supplementary Table 1 for molecular weights and actinide content. **c**, General strategy for the formation of single crystals of actinide–POM complexes and their spectroscopic and structural characterization, using as little as 1–10 µg actinide. The actinide–POM complexes were first formed in situ, followed by the addition of the Rb^+ or Cs^+ counter ions to allow for the crystallization of the actinide–POM alkali salt. The use of Rb^+ or Cs^+ also increases further the molecular weight of the compound, hence reducing the final percentage of actinide in the crystals. The four photographs show, from left to right, an aqueous sample of Cm–PW_{11} following crystallization (note the lack of Cm^{3+} emission from the Cm-depleted solution), dendritic crystals of $Cm(BW_{11})_2$, single crystals of $Cm(PW_{11})_2$ in crystallography oil and a single crystal of $Cm(BW_{11})_2$ during SCXRD measurement. The four photographs were taken under UV light irradiation. The crystals are transparent and non-fluorescent under ambient light.

characteristics, very few transneptunium–POM compounds have been structurally characterized: only the PuO_2^{2+}–$GeW_9O_{34}^{10-}$ and An^{4+}–$P_2W_{17}O_{61}^{10-}$ (An = Pu, Am) complexes[24,25], and all from milligram quantities of actinide (Supplementary Table 1). Information on transplutonium elements with POMs is even rarer[26,27], with only a handful of pioneering studies on Am^{3+} and Cm^{3+} with $P_5W_{30}O_{110}^{15-}$, $PW_{11}O_{39}^{7-}$, $SiW_{11}O_{39}^{8-}$ and $P_2W_{17}O_{61}^{10-}$ using cyclic voltammetry[28,29] and fluorescence spectroscopy[30]. The heavy nature of POMs has never been leveraged to crystallize complexes of rare isotopes while using minute amounts of material. Here we demonstrate that POMs enable both the spectroscopic and structural characterization of rare radioisotopes. Several curium–heteropolytungstate complexes ($Cm(W_5O_{18})_2^{9-}$, $CmPW_{11}O_{39}^{4-}$, $Cm(PW_{11}O_{39})_2^{11-}$, $CmBW_{11}O_{39}^{6-}$, $Cm(BW_{11}O_{39})_2^{15-}$, $CmP_2W_{17}O_{61}^{7-}$ and $Cm(P_2W_{17}O_{61})_2^{17-}$), along with their $^{243}Am^{3+}$ and lanthanide analogues, have been characterized in solution and the solid state (steady-state and time-resolved fluorescence, UV-visible-near infrared (NIR) spectrophotometry, ^{31}P NMR spectroscopy and Raman microscopy). Finally, we show that single crystals can reliably be obtained from 1–10 µg of actinide (Fig. 1c), providing the first three actinide(III)–POM SCXRD structures and an experimental evaluation of the eight-coordinated ionic radius of Cm^{3+}.

Results and discussion

Light polyoxotungstate–actinide complexes. Among the range of POMs that are known to bind cations[31–34], we selected the polyoxotungstates because of their high molecular weight, aqueous solubility and ease of preparation. The simplest, $W_5O_{18}^{6-}$ (W_5), is compatible with actinide aqueous chemistry as it assembles following the dissolution of Na_2WO_4 at pH values in the range of ~2 to ~7 in the presence of metal ions. The effective complexation of Cm^{3+} by W_5 was first confirmed by fluorescence spectroscopy (Fig. 2b–d). Addition of W_5 to an acetate-buffered solution of Cm^{3+} triggered an ~400-fold increase in curium luminescence, a large shift in the emission maximum (598.4 to 604.6 nm) and splitting into multiple Stark levels (582.6, 598.0, 604.6, 613.6 and 633.6 nm; Supplementary Fig. 1) due to the ligand field. Based on previous studies on lanthanides[35,36], the formation of the sandwich-type complex $[M^{III}(W_5O_{18})_2]^{9-}$ ($M(W_5)_2$) was expected. The $Cm(W_5)_2$ samples appeared intensely bright orange under UV light, even when containing submicrogram amounts of Cm^{3+} (Supplementary Figs. 2–4). The quantum yield of $Cm(W_5)_2$ was determined to be 17.9% in aqueous solution, similar to the most efficient organic ligands[37,38] that sensitize curium. W_5 was also found to sensitize Eu^{3+}, Tb^{3+}, Sm^{3+} and Dy^{3+} (Fig. 2a), but the brightest, $Eu(W_5)_2$, has a quantum

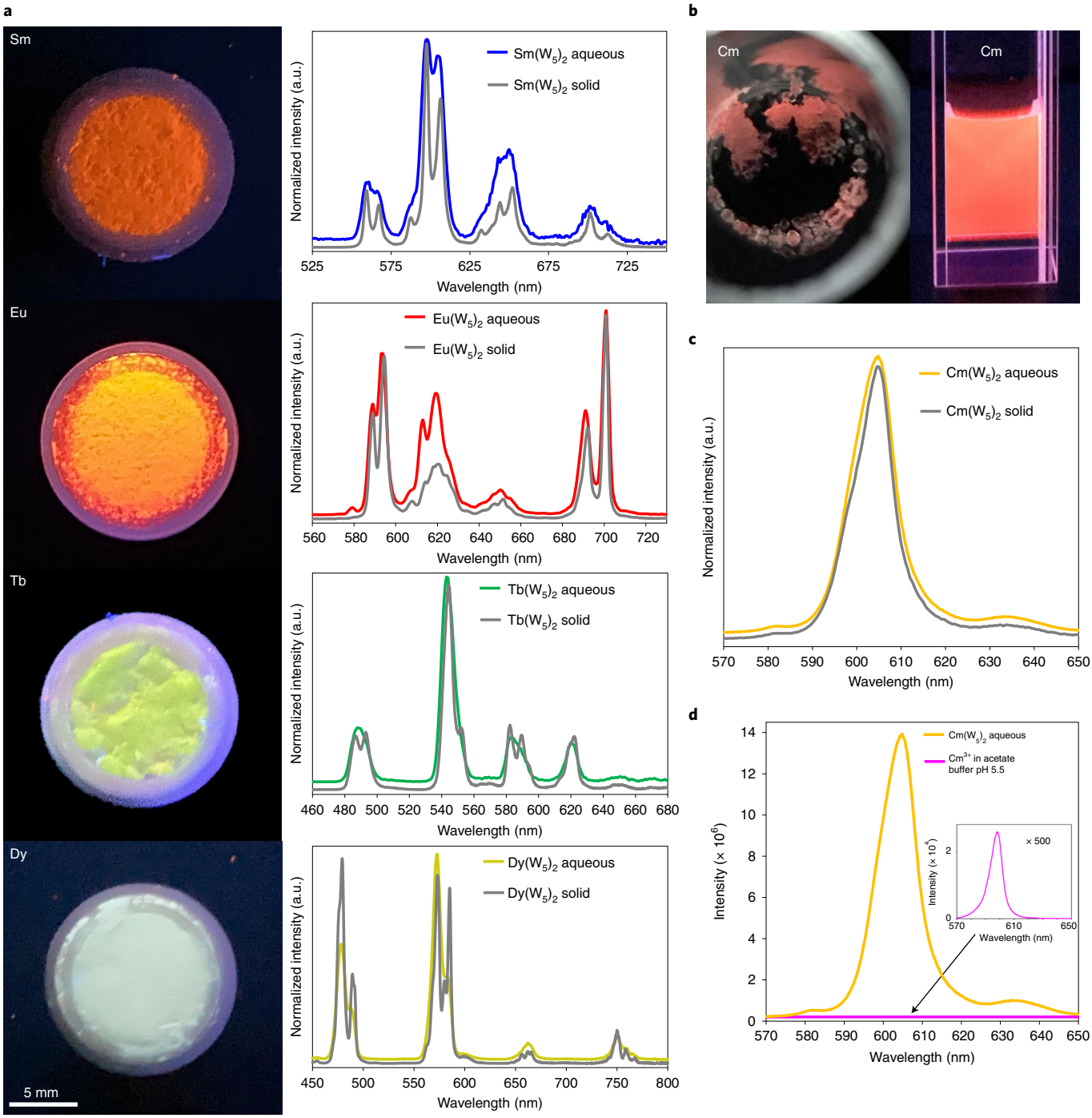

Fig. 2 | Luminescence properties of the W_5 POM complexes with trivalent lanthanide and curium ions. a, Photographs of solid samples of $Ln(W_5)_2$ (Ln = Sm, Eu, Tb, Dy) under UV light showing the sensitization properties of the POM and their emission spectra in the solid state and in solution, showing the similarity of the solid- and solution-state emission. **b**, Photographs of solid $Cm(W_5)_2$ (mass of $^{248}Cm = 3\,\mu g$) co-precipitated with CsCl–CH_3COOCs (from the initial buffer; left) and an aqueous solution of $Cm(W_5)_2$ (right) both under UV light. **c**, Comparison of the emission spectra of $Cm(W_5)_2$ in the solid state and in solution. **d**, Comparison of the emission spectra of unchelated Cm^{3+} (in acetate buffer) and $Cm(W_5)_2$, showing the substantial increase in luminescence upon complexation by the POM. The inset shows the luminescence of unchelated Cm^{3+} scaled by a factor of 500. [Cm] = 20 μM, [W_5] = 0 or 40 μM. Additional photographs of the luminescent $Cm(W_5)_2$ samples are provided in Supplementary Figs. 2–4.

yield of only 5.0% (0.18, 0.70 and 0.33% for Tb, Sm and Dy, respectively; Supplementary Figs. 5–8). Given the brightness of $Cm(W_5)_2$, we were also able to safely measure its fluorescence properties in the solid state, using ~60 ng ^{248}Cm, deposited onto a sample holder by simple evaporation of an aqueous drop of $Cm(W_5)_2$. Comparison of the solution and solid-state emission spectra (Fig. 2c) as well as the excitation spectra (Supplementary Fig. 9) indicates that the coordination of $Cm(W_5)_2$ remains similar upon crystallization.

Crystallization of $Ln(W_5)_2$ and $Cm(W_5)_2$ was attempted by leveraging the lower solubility of tungstate POMs in the presence of larger alkali ions[39]. Crystallization tests were performed using Cs^+ and Rb^+ to both decrease the POM solubility and increase the

molecular weight of the compound to 3,200–3,600 g mol^{-1}. The addition of CsCl or RbCl to $Cm(W_5)_2$ solutions reliably yielded fluorescent crystals characteristic of $Cm(W_5)_2$ within a few days. However, when using ~10 µg $^{248}Cm^{3+}$, only microcrystals that were too small to analyse with a benchtop SCXRD instrument were obtained (Supplementary Fig. 2). Conversely, successful crystallization of $Eu(W_5)_2$ and $Nd(W_5)_2$ was achieved when increasing the amount to 1–2 mg. The SCXRD structures confirmed the formation of the sandwich-type complex under the studied conditions, with the central Ln^{3+} being eight-coordinated (Supporting Information).

Heavier polyoxotungstate–actinide complexes. Although single crystals suitable for X-ray diffraction (XRD) were not obtained for $Cm(W_5)_2$ at the microscale, we did not pursue their synthesis using higher amounts of this extremely rare isotope because our goal was to obtain absolute structural information from microgram quantities. However, these results provided a guiding principle for the POM-based strategy and the study was extended to heavier POM complexes (>4,000 g mol^{-1}; Fig. 1). The lacunary Keggin (PW_{11} and BW_{11}) and Wells–Dawson (P_2W_{17}) POMs fit this criterion and can be reliably synthesized. The spontaneous in situ complexation of PW_{11}, BW_{11} and P_2W_{17} to actinides in aqueous solution and at room temperature was first confirmed for $^{243}Am^{3+}$ by spectrophotometry through its chelation-sensitive *f*–*f* absorbance band[40] at ~500 nm (Fig. 3a–e). Interestingly, these heavier POMs (relative to W_5) form at least two aqueous species with distinct absorbance properties (Supplementary Table 2). On addition of 1 equiv. of POM, the Am^{3+} absorbance band shifts from 504 to 508–512 nm, which we ascribe to the 1:1 complexes $[Am(BW_{11}O_{39})(H_2O)_x]^{6-}$, $[Am(PW_{11}O_{39})(H_2O)_x]^{4-}$ and $[Am(P_2W_{17}O_{61})(H_2O)_x]^{7-}$. Further addition of POM shifts the peak to 512–520 nm, corresponding to the formation of $[Am(BW_{11}O_{39})_2(H_2O)_x]^{15-}$ ($Am(BW_{11})_2$), $[Am(PW_{11}O_{39})_2(H_2O)_x]^{11-}$ ($Am(PW_{11})_2$) and $[Am(P_2W_{17}O_{61})_2(H_2O)_x]^{17-}$ ($Am(PW_{11})_2$). These observations are also supported by the existence of two ^{31}P NMR signals, corresponding to the 1:1 and 1:2 complexes in both Am–PW_{11} and Eu–PW_{11} solutions (Supplementary Fig. 10). Substantial shifts in the absorbance of Cm^{3+} also confirmed its in situ chelation with these POMs (Fig. 3f). These results were further confirmed with Nd^{3+} and Er^{3+} (Supplementary Figs. 11–13).

The three selected POMs were further characterized by steady-state and time-resolved fluorescence spectroscopy (Fig. 4). PW_{11}, BW_{11} and P_2W_{17} were found to sensitize Eu^{3+} by indirect excitation through the POM and intramolecular energy transfer (Fig. 4c,d). The brightness of the $Eu(POM)_2$ species follows the trend $W_5 > PW_{11} > P_2W_{17} \approx BW_{11}$. Intensity aside, the emission spectra of $Eu(P_2W_{17})_2$, $Eu(PW_{11})_2$ and $Eu(BW_{11})_2$ in aqueous solution are very similar, but depart from that of $Eu(W_5)_2$, suggesting distinct coordination environments for Eu^{3+} with PW_{11}, BW_{11} and P_2W_{17} compared with $Eu(W_5)_2$. The versatility of the POM-based chelating platform is manifested in the excitation spectra of Eu^{3+}, as the POM series displays a tunable excitation energy, with maxima at 325, 315, 295 and 270 nm for $Eu(P_2W_{17})_2$, $Eu(PW_{11})_2$, $Eu(BW_{11})_2$ and $Eu(W_5)_2$, respectively (Fig. 4d). Consistent with the spectrophotometric and NMR results obtained with the Am–POMs, the fluorescence signature of the Eu–POM samples reveals the sequential formation of the 1:1 and 1:2 complexes upon addition of the POM (Supplementary Fig. 14 and Supplementary Table 3).

PW_{11}, BW_{11} and P_2W_{17} also efficiently sensitize Cm^{3+}. In situ complexation to these POMs shifts the Cm^{3+} emission from 598.4 to 601.6, 601.2 and 601.6 nm for PW_{11}, BW_{11} and P_2W_{17}, respectively (Fig. 4a). Similar to Eu^{3+}, the emission spectra of $Cm(PW_{11})_2$, $Cm(BW_{11})_2$ and $Cm(P_2W_{17})_2$ are very similar to each other but differ from that of $Cm(W_5)_2$ ($\lambda_{max} = 604.6$ nm). The excitation spectra of Cm^{3+} further evidence its complexation by PW_{11}, BW_{11} and P_2W_{17}, even at micromolar concentrations, with all sensitizing Cm^{3+} luminescence through their excited state at ~260 nm, as opposed to the direct excitation of Cm^{3+}, which occurs at ~396 nm (Fig. 4b). The excitation energies of the Cm–POMs are different from those of the Eu–POMs (vide supra), which is a first indication that the speciation of Cm^{3+} and Eu^{3+} with PW_{11}, BW_{11} and P_2W_{17} in aqueous solution may not be identical.

Time-resolved fluorescence measurements revealed long lifetimes for solutions of Eu–P_2W_{17}, Eu–PW_{11}, Eu–BW_{11} and Eu–W_5 of 2,300–3,200 µs (Fig. 4f and Supplementary Table 3). Based on Kimura's widely used empirical equations[41], these long lifetimes indicate that no water molecule is coordinated to Eu^{3+} in the $Eu(POM)_2$ species and imply the formation of sandwich-type eight-coordinated complexes (consistent with the obtained crystal structures, vide infra). By contrast, Cm^{3+} exhibits a long lifetime (780 ± 5 µs) only when bound to W_5. As shown in Fig. 5a, $Cm(W_5)_2$ exhibits the longest luminescence lifetime observed for an aqueous Cm^{3+} complex, ~40% longer than the previous highest value. This remarkably long lifetime was confirmed for $Cm(W_5)_2$ in both the solid state and in aqueous solution. Previously, long-lived Cm^{3+} emission has only been observed in the solid state and with Cm^{3+}-doped minerals[42,43], with multidentate organic chelators in solution leading to only moderately long lifetimes. W_5 therefore combines the optimum properties of multidentate water-soluble ligands and minerals. Using Kimura's equation[41], the 780 µs luminescence lifetime of $Cm(W_5)_2$ indicates that the lightest POM effectively shields Cm^{3+} from quenching water molecules, forming an eight-coordinated complex without H_2O. This is remarkable as most Cm^{3+} ions studied so far are nine-coordinated (Supplementary Table 1). Lifetime measurements for $Cm(W_5)_2$ in H_2O–D_2O mixtures (Supplementary Figs. 15 and 16) indicated a lifetime of 1,136 ± 57 µs in pure D_2O, almost matching the maximum value expected from Kimura's equation in a completely non-quenching environment (1,200 µs)[41].

The lifetimes of Cm–PW_{11}, Cm–BW_{11} and Cm–P_2W_{17} in solution are all short: 87, 90 and 87 µs, respectively (Fig. 4e). Despite evidence of complexation (from emission, excitation and UV-visible spectra, analogous to Am^{3+}), the lifetimes for POM–Cm^{3+} in solution remain short, even when using superstoichiometric ratios of POM/Cm (Supplementary Table 4 and Supplementary Figs. 17 and 18). Interestingly, a previous study[30] reported, without further interpretation, lifetimes in the range of 60–100 µs for Cm–PW_{11} and Cm–$SiW_{11}O_{39}^{8-}$ solutions (in 0.1–0.5 M HNO_3). The short lifetimes of Cm^{3+} with PW_{11}, BW_{11} and P_2W_{17} contrast the behaviour observed for $Cm(W_5)_2$, and also reveal a notable difference between the Cm^{3+} and Eu^{3+} complexes (Fig. 4e,f). These short lifetimes would correspond to six to nine coordinating water molecules, based on Kimura's equation, at odds with the expected metal coordination (Fig. 1), suggesting that this widely used model, developed with a basis set of mainly Cm^{3+} carboxylate lifetimes[44], is not applicable to all POM–Cm^{3+} species. Dynamic equilibrium with the solvent, or quenching by the POM ions, or both, is also possible. Furthermore, substantial changes in the fluorescence properties of $Cm(PW_{11})_2$ and $Cm(BW_{11})_2$ were observed upon transition from solution to the solid state. After crystallization by evaporation followed by drying (Fig. 5b,c), the emission maxima of $Cm(PW_{11})_2$ and $Cm(BW_{11})_2$ shift from 601.6 to 607.2 and 609.8 nm, respectively, indicating that distinct species form in solution and the solid state. The excitation maximum of $Cm(BW_{11})_2$ also shifts from 260 to 295 nm, close to the value observed for $Eu(BW_{11})_2$ (Supplementary Fig. 19). Additionally, a notable increase in the lifetime was observed, rising from ~90 µs in solution to 257 and 225 µs in the solid state for $Cm(PW_{11})_2$ and $Cm(BW_{11})_2$, respectively. These lifetimes would correspond to two to three water molecules based on Kimura's equation, but solid-state characterization suggests otherwise (vide infra), further indicating that this model is not suitable for Cm^{3+} complexes with PW_{11}, BW_{11} and P_2W_{17}.

Isolation and solid-state characterization of transplutonium complexes at the microscale. For a given mass of actinide, PW_{11}

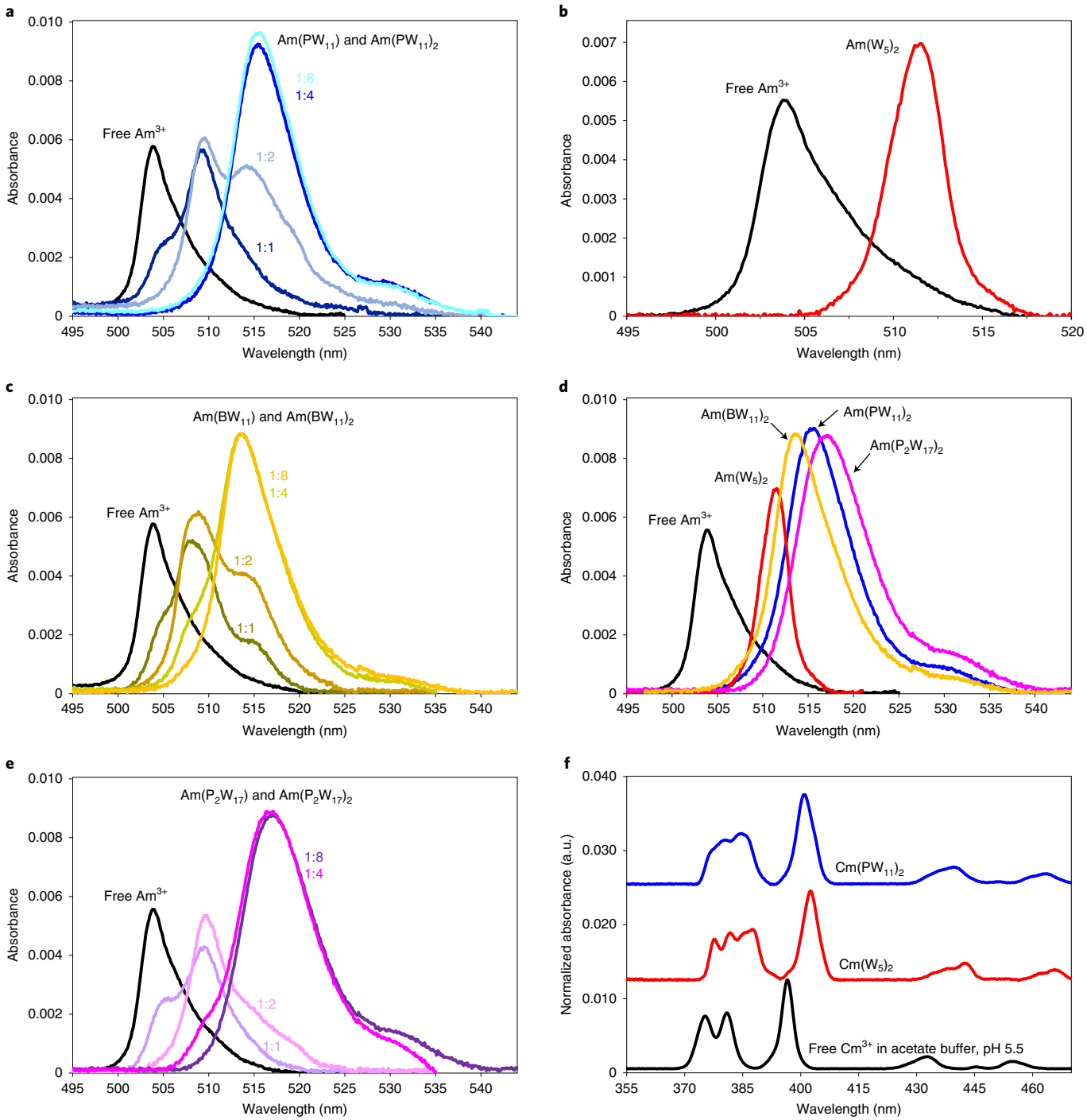

Fig. 3 | Absorbance properties of americium and curium ions upon complexation with POMs. a, Absorbance spectra of solutions containing the POM PW_{11} and trivalent americium, showing the sequential formation of 1:1 and 1:2 Am–POM species. The total concentration ratio Am/POM was varied from 0 (free Am^{3+}) to 1:8, as indicated above each spectrum. [Am] = 15 μM, [POM] = 0, 15, 30, 60 or 120 μM, pH 5.5 (acetate buffer). **b**, Detailed comparison of the absorbance spectra of free Am^{3+} and the complex $Am(W_5)$. **c**, The absorbance spectra from similar experiments to **a** but with the POM BW_{11}. **d**, Comparison of the absorbance spectra of the different $Am(POM)_2$ complexes formed with W_5, PW_{11}, BW_{11} and P_2W_{17}. **e**, The absorbance spectra from similar experiments to **a** but with the POM P_2W_{17}. **f**, Comparison of the absorbance data observed with uncomplexed Cm^{3+} and the complexes $Cm(W_5)_2$ and $Cm(PW_{11})_2$. Analogous results for the lanthanides Nd^{3+} and Er^{3+} are given in Supplementary Figs. 8 and 9.

and BW_{11} yielded larger crystals than W_5. It was possible to analyse the solid samples by Raman microscopy (Fig. 5d) because the actinide–POM crystals contain only a minimal amount of the radioisotope (Fig. 1a) and are safer to handle than small-ligand complexes. Visual inspection confirmed the crystallinity of the materials. Comparison of the Raman spectra of the ^{243}Am- and ^{248}Cm-containing crystals and the starting materials confirmed the reactions and that no co-crystallized reactants were present in the crystals (Supplementary Figs. 20 and 21).

Although $Cm(W_5)_2$ crystals were too small for SCXRD (Supplementary Fig. 2), Raman spectroscopy further confirmed the complexation of Cm^{3+} by W_5 and allowed identification of

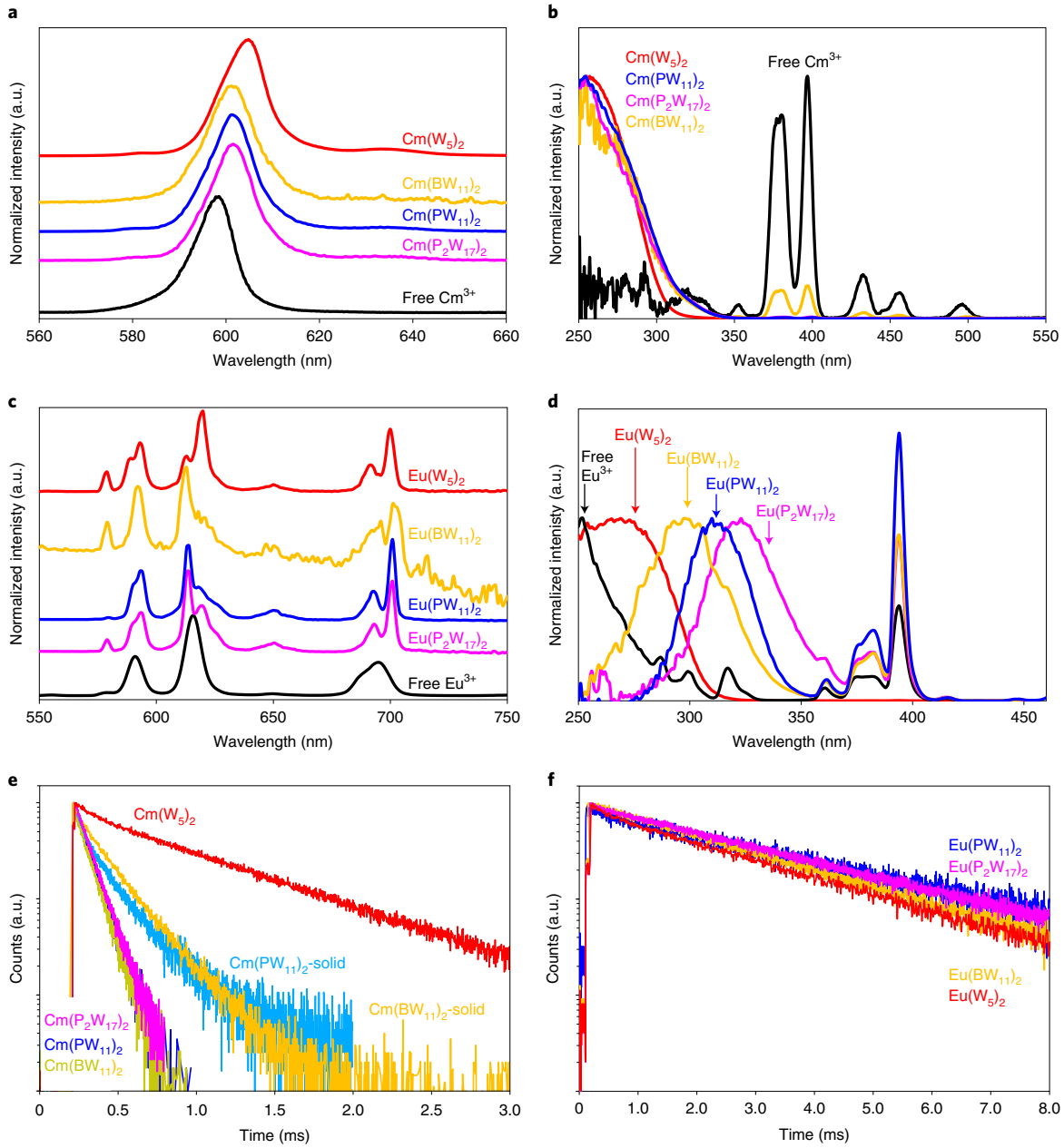

Fig. 4 | Steady-state and time-correlated fluorescence properties of lanthanide–POM and curium–POM complexes. a,**b**, Emission (**a**) and excitation (**b**) spectra of a series of curium–POM complexes, and comparison with unbound Cm^{3+} in solution at pH 5.5 (0.1 M acetate buffer). The largest emission shift is observed in the presence of the smaller POM, that is, W_5. Note the similarity of the spectra of the BW_{11}, PW_{11} and P_2W_{17} complexes of curium. **c**,**d**, Emission (**c**) and excitation (**d**) spectra of the equivalent europium–POM complexes, and comparison with unbound Eu^{3+} in solution. Also note the similarity of the spectra of the BW_{11}, PW_{11} and P_2W_{17} complexes of europium. **e**, Fluorescence lifetime decay curves of the Cm–POM complexes in solution and the solid state, as indicated on the graph. The fluorescence lifetime of Cm^{3+} in the presence of W_5 is long (780 μs), whereas the fluorescence lifetime of Cm^{3+} in the presence of BW_{11}, PW_{11} or P_2W_{17} is short in solution, despite the evidence of complexation and the formation of 1:2 complexes. **f**, Fluorescence lifetime decay curves of the Eu–POM complexes in solution. In contrast to curium, the lifetime of europium is long in the presence of the four POMs tested.

the compound (Supplementary Fig. 20). The Raman spectrum of $Cm(W_5)_2$, formulated $Rb_9[Cm(W_5O_{18})_2]\cdot nH_2O$, features an intense band at 968.5 cm^{-1} (W=O terminal), a weak double band at 825–875 cm^{-1} (W–O–W) and multiple bands at 50–300 cm^{-1}, in line with the data reported[45,46] for $Eu(W_5O_{18})_2^{9-}$ and almost identical to, but slightly shifted compared with the Raman spectrum[36] of $Na_8[Th(W_5O_{18})_2]\cdot 28H_2O$.

$Cm(PW_{11})_2$, $Cm(BW_{11})_2$, $Am(BW_{11})_2$ and $Am(PW_{11})_2$ were successfully isolated by crystallization, even when using amounts of ^{248}Cm or ^{243}Am as low as 1–10 μg, and could certainly be scaled-down further (Fig. 6, Supplementary Figs. 3, 4, 20 and 21, and Materials and methods). As there was little information available on BW_{11} in the literature, we performed a systematic study of this particular POM with several lanthanides using the same crystallization conditions as used for curium and americium (Supplementary Fig. 22). The Raman spectra of $Am(BW_{11})_2$ and $Cm(BW_{11})_2$ present the same features as observed with the lanthanides, with a double band at 966–952 cm^{-1} (W=O terminal), a weak band at 897 cm^{-1} (W–O–W)

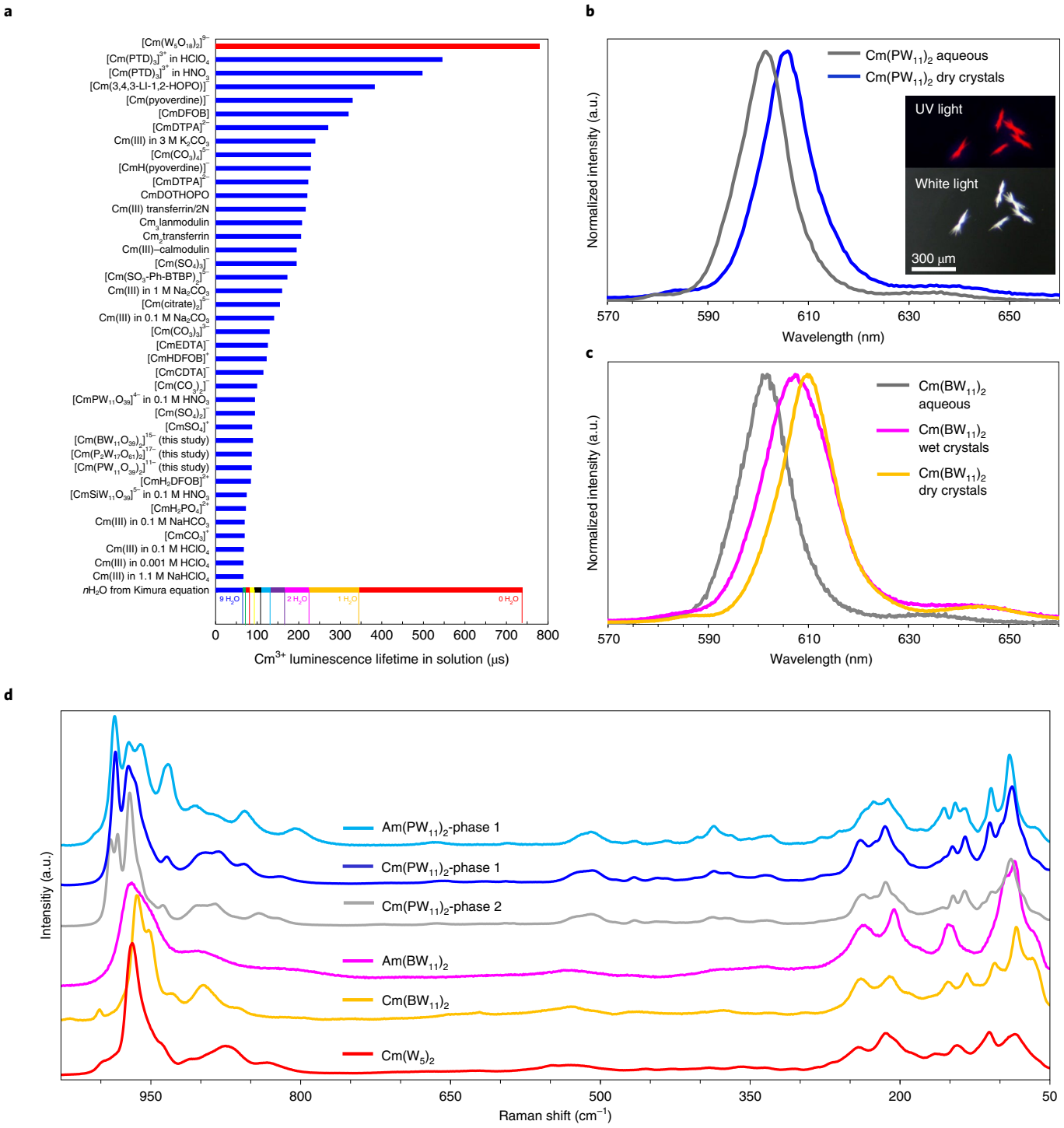

Fig. 5 | Luminescence lifetimes of Cm^{3+} complexes in solution and Cm–POM transition from solution to the solid state. a, Comparison of the luminescence lifetimes of $Cm(W_5)_2$, $Cm(BW_{11})_2$, $Cm(PW_{11})_2$ and $Cm(P_2W_{17})_2$ with previously reported luminescent Cm^{3+} complexes. $Cm(W_5)_2$ has the longest lifetime (780 μs) reported for a Cm^{3+} complex. Numerical values of the lifetimes are given in Supplementary Table 5. **b**,**c**, Comparison of the fluorescence emission in the solid state and in aqueous solution for the $Cm(PW_{11})_2$ (**b**) and $Cm(BW_{11})_2$ (**c**) complexes. The inset in **b** shows photographs of $Cm(PW_{11})_2$ crystals under UV and white light. **d**, Raman spectra of $Cm(W_5)_2$, $Cm(BW_{11})_2$, the two isomers of $Cm(PW_{11})_2$, $Am(BW_{11})_2$ and $Am(PW_{11})_2$ in the solid state. The Raman spectra of the Cm–POMs and Am–POMs are compared with the spectra of the corresponding starting POMs in Supplementary Figs. 20 and 21.

and moderately intense bands below 250 cm^{-1} (Fig. 5d). A slightly increased shift of the band at ~530 cm^{-1} (bending O–B–O)[47] can also be observed within the $Ln(BW_{11})_2$ series, and bands of $Am(BW_{11})_2$ and $Cm(BW_{11})_2$ fall in the expected range.

For PW_{11} with curium, the Raman analysis revealed the presence of two distinct phases, depending on the crystal or even on which part of the sample was analysed (for polycrystalline aggregates, see Supplementary Fig. 23). The Raman spectra of the two Cm–PW_{11}

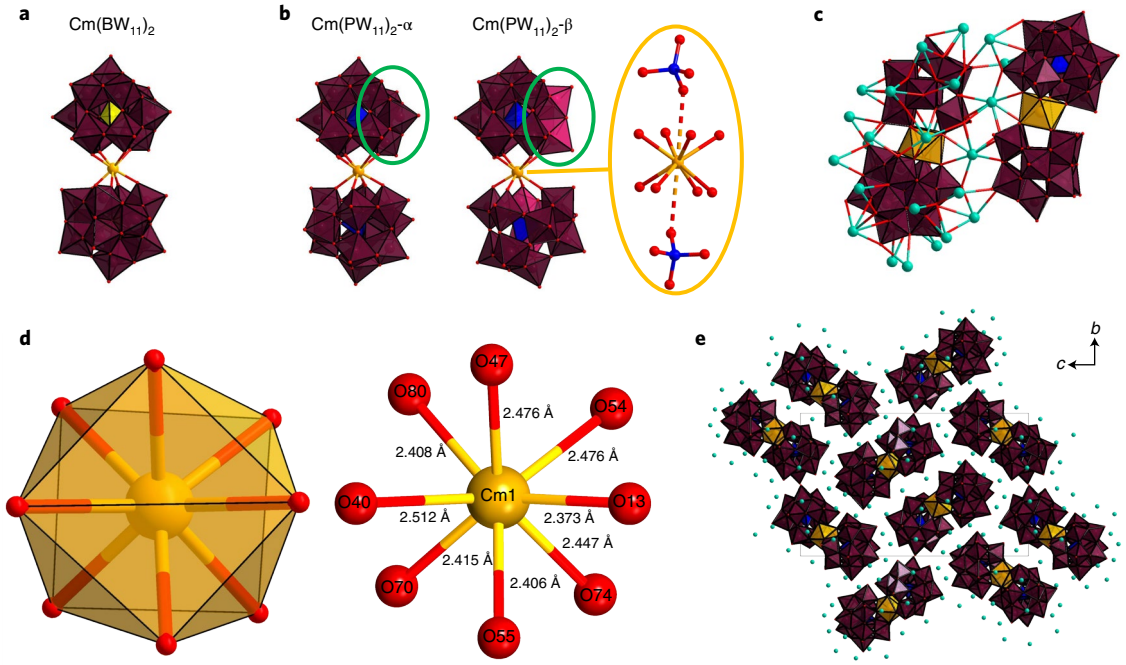

Fig. 6 | SCXRD structures of transplutonium element complexes with POMs. a, Structure of the Cm^{3+} complex with the POM BW_{11}, denoted $Cm(BW_{11})_2$. Full formula: $Cs_{13}H_2Cm(BW_{11}O_{39})_2 \cdot 13H_2O$. **b**, Structures of the two complexes isolated from Cm^{3+} and the POM PW_{11}. One of the complexes contains the α-isomer of the Keggin POM, namely $Cm(PW_{11})_2$-α. Full formula: $Cs_{11}Cm(\alpha\text{-}PW_{11}O_{39})_2 \cdot 18H_2O$. The other complex contains the β-isomer of the Keggin POM, namely $Cm(PW_{11})_2$-β. Full formula: $Cs_{11}Cm(\beta\text{-}PW_{11}O_{39})_2 \cdot 31.5H_2O$. The green ellipses highlight the difference between the α- and β-isomers of the Keggin ion. A detailed view of the ten O atoms nearest to Cm^{3+} in $Cm(PW_{11})_2$-β is presented in the yellow ellipse. **c**, View of $Cm(PW_{11})_2$-α, highlighting the positions of the Cs^+ ions. The Cs^+ ions both bridge the Cm–POM complexes, promoting crystallization, and create a cage around the equatorial plane, shielding Cm^{3+} from solvent molecules. The Cs–O_{POM} bond lengths are in the range 2.7–3.8 Å. **d**, First coordination sphere of Cm^{3+} in $Cm(PW_{11})_2$-α. **e**, View along the *a* axis of $Cm(PW_{11})_2$-α, highlighting the arrangement of pairs of $Cm(PW_{11})_2$-α in the lattice. Colour code: orange, Cm; maroon, W, with rotated trimer in pink for $Cm(PW_{11})_2$-β; blue, P; yellow, B; red, O; cyan, Cs. Additional views of the three Cm–POMs are given in Supplementary Figs. 25–27.

phases differ from the starting material but are similar to each other, the main difference being the splitting and position of the bands at 950–1,000 cm^{-1}, indicating that two Cm–polyoxotungstate isomers could have formed (Fig. 5d). With americium, only one phase was obtained, identified as $Am(PW_{11})_2$-α based on its Raman spectrum (Fig. 5d and Supplementary Fig. 21). Likewise, only the α-isomer was observed for the lanthanides, for which we obtained six SCXRD structures: $Ln(PW_{11})_2$-α and $Ln(BW_{11})_2$ with Nd^{3+}, Eu^{3+} and Sm^{3+} (Supplementary Table 6).

The $Cm(BW_{11})_2$ and $Cm(PW_{11})_2$ complexes were further characterized by SCXRD, providing definitive evidence that the two distinct Raman spectra seen for $Cm(PW_{11})_2$ arise from the crystallization of two isomers of the Keggin structure, namely $Cm(PW_{11})_2$-α and $Cm(PW_{11})_2$-β (Fig. 6).

$Cm(PW_{11})_2$-α, fully formulated as $Cs_{11}[Cm(PW_{11}O_{39})_2] \cdot 18H_2O$, crystallizes in the monoclinic space group $P2_1/c$ ($V = 9013.5(5)$ Å^3). The second phase, $Cm(PW_{11})_2$-β, formulated as $Cs_{11}[Cm(PW_{11}O_{39})_2] \cdot 31.5H_2O$, crystallizes in the monoclinic space group $P2_1/n$ ($V = 10488.2(6)$ Å^3). These structures feature two tetradentate $PW_{11}O_{39}^{7-}$ ions complexing a central eight-coordinated square-antiprismatic Cm^{3+} ion with Cm–O bond lengths in the range 2.37–2.52 Å. $Cm(PW_{11})_2$-β features elongated P–O bonds: 1.56(2)–1.923(13) Å compared with 1.513(13)–1.554(13) Å for $Cm(PW_{11})_2$-α. The single phase of $Cm(BW_{11})_2$, formulated as $Cs_{13}H_2[Cm(BW_{11}O_{39})_2] \cdot 13H_2O$, crystallizes in the monoclinic space group $P2_1/c$ ($V = 9654.08(6)$ Å^3). It features two $BW_{11}O_{39}^{9-}$ anions complexing Cm^{3+} with an eight-fold square-antiprismatic coordination, Cm–O bond lengths in the range 2.411(10)–2.475(12) Å and no coordinated H_2O. The presence of 13 alkali ions and two protons was observed across all four $M(BW_{11})_2$ structures obtained (M = Cm^{3+}, Nd^{3+}, Sm^{3+}, Eu^{3+}), consistent with the protonation state of unbound BW_{11} observed[48] in solution. Beside the eight coordinating oxygen atoms of the two tungstate cages, the next-closest oxygen atoms are from the two encapsulated phosphate or borate ions, with Cm–O distances of 3.47(2), 3.49(4) and 3.62(3) Å for $Cm(PW_{11})_2$-α, $Cm(PW_{11})_2$-β and $Cm(BW_{11})_2$, respectively (Fig. 6c). We hypothesize that the phosphate or borate ions remain partially flexible within their rigid tungstate cages[49], providing a relaxation mechanism and leading to short lifetimes, even in the solid state (vide supra).

The three Cm–POM structures reported herein represent the first actinide(III)–polyoxometalates to be characterized, and feature the heaviest element complexed to a polyoxoanion. Consistent with the eight-coordinated geometry, the Cm–O distances in the Cm–POMs are slightly shorter (average: 2.44(4) Å) than those reported for nine- and ten-coordinated Cm^{3+}–ligand compounds previously obtained from milligram quantities[10,50–52]. One eight-coordinated curium compound has previously been reported[53], $Cm(IO_3)_3$, but its polyhedral is highly distorted due to eight binding IO_3^- ligands (Cm–O distances of 2.32–2.57 Å), precluding evaluation of the ionic radii. Using these Cm–POM structures, those of six analogous Ln–POM complexes (Supplementary Table 6) and Shannon's ionic radii for Ln^{3+} ions[54], we determined an ionic radius of 1.099(10) Å for the eight-coordinated Cm^{3+}. This value is slightly larger than the only eight-coordinated ionic radius for a trivalent actinide reported by Shannon[54], 1.09 Å for Am^{3+} (based on a single and distorted structure[55]), but is consistent with the more recent measurement by Cross et al.[56] (1.108 Å for Am^{3+}). These results indicate that, among the lanthanides, promethium (Pm^{3+}) is the closest size-match for Cm^{3+} (Supplementary Fig. 24).

Conclusions

In this study we leveraged POMs as a convenient tool to capture and study the coordination chemistry of hazardous and/or expensive radioisotopes. POM-based chelation allows for a better use of these precious materials, minimizes workers' exposure and opens a novel avenue to investigate elusive elements. Given the wide variety of POMs that exist (for example, tungstates, molybdates, tantalates, Keggin, Wells–Dawson and Preyssler ions), the strategy could be applied to obtain several SCXRD structures of transuranic elements while respecting the low isotope availability. The POM-based strategy also likely represents the most promising route to prepare and characterize compounds of elements for which no SCXRD structure has ever been obtained, notably einsteinium and actinium.

Online content

Any methods, additional references, Nature Research reporting summaries, source data, extended data, supplementary information, acknowledgements, peer review information; details of author contributions and competing interests; and statements of data and code availability are available at https://doi.org/10.1038/s41557-022-01018-8.

Received: 20 December 2021; Accepted: 4 July 2022;
Published online: 01 September 2022

References

1. Roberto, J. B. et al. Actinide targets for the synthesis of super-heavy elements. *Nucl. Phys. A* **944**, 99–116 (2015).
2. McMillan, E. & Abelson, P. H. Radioactive element 93. *Phys. Rev.* **57**, 1185–1186 (1940).
3. Seaborg, G. T. The transuranium elements. *Science* **104**, 379–386 (1946).
4. Groom, C. R., Bruno, I. J., Lightfoot, M. P. & Ward, S. C. The Cambridge Structural Database. *Acta Crystallogr. B* **72**, 171–179 (2016).
5. Arnold, P. L., Dutkiewicz, M. S. & Walter, O. Organometallic neptunium chemistry. *Chem. Rev.* **117**, 11460–11475 (2017).
6. *NIST Inorganic Crystal Structure Database (ICSD)* (NIST, 2020); https://doi.org/10.18434/M32147
7. Silver, M. A. et al. Characterization of berkelium(III) dipicolinate and borate compounds in solution and the solid state. *Science* **353**, aaf3762 (2016).
8. Silver, M. A. et al. Electronic structure and properties of berkelium iodates. *J. Am. Chem. Soc.* **139**, 13361–13375 (2017).
9. Galley, S. S. et al. Synthesis and characterization of tris-chelate complexes for understanding *f*-orbital bonding in later actinides. *J. Am. Chem. Soc.* **141**, 2356–2366 (2019).
10. Sperling, J. M. et al. Compression of curium pyrrolidine-dithiocarbamate enhances covalency. *Nature* **583**, 396–399 (2020).
11. Goodwin, C. A. P. et al. Isolation and characterization of a californium metallocene. *Nature* **599**, 421–424 (2021).
12. Ferrier, M. G. et al. Synthesis and characterization of the actinium aquo ion. *ACS Cent. Sci.* **3**, 176–185 (2017).
13. Deblonde, G. J.-P., Zavarin, M. & Kersting, A. B. The coordination properties and ionic radius of actinium: a 120-year-old enigma. *Coord. Chem. Rev.* **446**, 214130 (2021).
14. Thiele, N. A. & Wilson, J. J. Actinium-225 for targeted α therapy: coordination chemistry and current chelation approaches. *Cancer Biother. Radiopharm.* **33**, 336–348 (2018).
15. Kelley, M. P. et al. Revisiting complexation thermodynamics of transplutonium elements up to einsteinium. *Chem. Commun.* **54**, 10578–10581 (2018).
16. Deblonde, G. J.-P., Ricano, A. & Abergel, R. J. Ultra-selective ligand-driven separation of strategic actinides. *Nat. Commun.* **10**, 2438 (2019).
17. Carter, K. P. et al. Structural and spectroscopic characterization of an einsteinium complex. *Nature* **590**, 85–88 (2021).
18. Nugent, L. J., Baybarz, R. D., Werner, G. K. & Friedman, H. A. Intramolecular energy transfer and sensitized luminescence in an einsteinium β-diketone chelate and the lower lying electronic energy levels of Es(III). *Chem. Phys. Lett.* **7**, 179–182 (1970).
19. Allred, B. E. et al. Siderocalin-mediated recognition, sensitization, and cellular uptake of actinides. *Proc. Natl Acad. Sci. USA* **112**, 10342–10347 (2015).
20. Deblonde, G. J.-P. et al. Chelation and stabilization of berkelium in oxidation state +IV. *Nat. Chem.* **9**, 843–849 (2017).
21. Cotruvo, J. A. Jr, Featherston, E. R., Mattocks, J. A., Ho, J. V. & Laremore, T. N. Lanmodulin: a highly selective lanthanide-binding protein from a lanthanide-utilizing bacterium. *J. Am. Chem. Soc.* **140**, 15056–15061 (2018).
22. Cook, E. C., Featherston, E. R., Showalter, S. A. & Cotruvo, J. A. Jr Structural basis for rare earth element recognition by *Methylobacterium extorquens* lanmodulin. *Biochemistry* **58**, 120–125 (2019).
23. Deblonde, G. J.-P. et al. Characterization of americium and curium complexes with the protein lanmodulin: a potential macromolecular mechanism for actinide mobility in the environment. *J. Am. Chem. Soc.* **143**, 15769–15783 (2021).
24. Copping, R. et al. Probing the 5*f* electrons in a plutonyl(VI) cluster complex. *Dalton Trans.* **29**, 5609–5611 (2009).
25. Sokolova, M. N. et al. Synthesis and structural examination of complexes of Am(IV) and other tetravalent actinides with lacunary heteropolyanion α_2-$P_2W_{17}O_{61}^{10-}$. *Inorg. Chem.* **48**, 9185–9190 (2009).
26. Auvray, T. & Matson, E. M. Polyoxometalate-based complexes as ligands for the study of actinide chemistry. *Dalton Trans.* **49**, 13917–13927 (2020).
27. Dufaye, M., Duval, S. & Loiseau, T. Trends and new directions in the crystal chemistry of actinide oxo-clusters incorporated in polyoxometalates. *CrystEngComm* **22**, 3549–3562 (2020).
28. Antonio, M. R., Williams, C. W. & Soderholm, L. Synthesis and characterization of actinide-exchanged Preyssler heteropolyanions $[AnP_5W_{30}O_{110}]^{n-}$ (An≡Th, Am, Cm). *J. Alloys Compd.* **271–273**, 846–849 (1998).
29. Chiang, M.-H., Soderholm, L. & Antonio, M. R. Redox chemistry of actinide ions in Wells−Dawson heteropolyoxoanion complexes. *Eur. J. Inorg. Chem.* **2003**, 2929–2936 (2003).
30. Ioussov, A. & Krupa, J. C. Luminescence properties and stability constants of curium(III) complexes with lacunary heteropolyanions $PW_{11}O_{39}^{7-}$ and $SiW_{11}O_{39}^{8-}$ in nitric acid solutions. *Radiochim. Acta* **78**, 97–104 (1997).
31. Blazevic, A. & Rompel, A. The Anderson–Evans polyoxometalate: from inorganic building blocks via hybrid organic–inorganic structures to tomorrows 'Bio-POM'. *Coord. Chem. Rev.* **307**, 42–64 (2016).
32. Colliard, I., Morrison, G., zur Loye, H.-C. & Nyman, M. Supramolecular assembly of U(IV) clusters and superatoms with unconventional countercations. *J. Am. Chem. Soc.* **142**, 9039–9047 (2020).
33. Gumerova, N. I. & Rompel, A. Polyoxometalates in solution: speciation under spotlight. *Chem. Soc. Rev.* **49**, 7568–7601 (2020).
34. Colliard, I. et al. Snapshots of Ce_{70} toroid assembly from solids and solution. *J. Am. Chem. Soc.* **143**, 9612–9621 (2021).
35. Peacock, R. D. & Weakley, T. J. R. Heteropolytungstate complexes of the lanthanide elements. Part I. Preparation and reactions. *J. Chem. Soc. A* 1836–1839 (1971).
36. Griffith, W. P. et al. Studies on polyoxo- and polyperoxometalates: part 7. Lanthano- and thoriopolyoxotungstates as catalytic oxidants with H_2O_2 and the X-ray crystal structure of $Na_8[ThW_{10}O_{36}]\cdot 28H_2O$. *J. Organomet. Chem.* **607**, 146–155 (2000).
37. Law, G.-L. et al. Circularly polarized luminescence of curium: a new characterization of the 5*f* actinide complexes. *J. Am. Chem. Soc.* **134**, 15545–15549 (2012).
38. Sturzbecher-Hoehne, M., Kullgren, B., Jarvis, E. E., An, D. D. & Abergel, R. J. Highly luminescent and stable hydroxypyridinonate complexes: a step towards new curium decontamination strategies. *Chem. Eur. J.* **20**, 9962–9968 (2014).
39. Misra, A., Kozma, K., Streb, C. & Nyman, M. Beyond charge balance: counter-cations in polyoxometalate chemsitry. *Angew. Chem. Int. Ed.* **59**, 596–612 (2020).
40. Grimes, T. S. et al. Influence of a heterocyclic nitrogen-donor group on the coordination of trivalent actinides and lanthanides by aminopolycarboxylate complexants. *Inorg. Chem.* **57**, 1373–1385 (2018).
41. Kimura, T., Nagaishi, R., Kato, Y. & Yoshida, Z. Luminescence study on solvation of americium(III), curium(III) and several lanthanide(III) ions in nonaqueous and binary mixed solvents. *Radiochim. Acta* **89**, 125–130 (2001).
42. Holliday, K. et al. Discriminating factors affecting incorporation: comparison of the fate of Eu^{3+}–Cm^{3+} in the Sr carbonate–sulfate system. *Dalton Trans.* **41**, 3642–3647 (2012).
43. Holliday, K. S. et al. Site-selective time resolved laser fluorescence spectroscopy of Eu and Cm doped $LaPO_4$. *Radiochim. Acta* **100**, 189–195 (2012).
44. Kimura, T., Choppin, G. R., Kato, Y. & Yoshida, Z. Determination of the hydration number of Cm(III) in various aqueous solutions. *Radiochim. Acta* **72**, 61–64 (1996).
45. Sousa, F. L. et al. Luminescent polyoxotungstoeuropate anion-pillared layered double hydroxides. *Eur. J. Inorg. Chem.* **2006**, 726–734 (2006).
46. Wang, Z. et al. Chemically responsive luminescent switching in transparent flexible self-supporting $[EuW_{10}O_{36}]^{9-}$-agarose nanocomposite thin films. *J. Mater. Chem.* **20**, 271–277 (2009).
47. Caliman, E., Dias, J. A., Dias, S. C. L. & Prado, A. G. S. Solvent effect on the preparation of $H_3PW_{12}O_{40}$ supported on alumina. *Catal. Today* **107–108**, 816–825 (2005).
48. Maksimovskaya, R. I. & Maksimov, G. M. Borotungstate polyoxometalates: multinuclear NMR structural characterization and conversions in solutions. *Inorg. Chem.* **50**, 4725–4731 (2011).

49. Yamase, T. & Ishikawa, E. Structural characterization of the brown six-electron-reduced form of dodecatungstoborate, $K_5[BW_{12}O_{37}(H_2O)_3]\cdot 13.5H_2O$. *J. Chem. Soc., Dalton Trans.* 1619–1627 (1996).
50. Cary, S. K. et al. Emergence of californium as the second transitional element in the actinide series. *Nat. Commun.* **6**, 6827 (2015).
51. Jones, Z. R. et al. Advancing understanding of actinide(III) (Ac, Am, Cm) aqueous complexation chemistry. *Chem. Sci.* **12**, 5638–5654 (2021).
52. Polinski, M. J. et al. Differentiating between trivalent lanthanides and actinides. *J. Am. Chem. Soc.* **134**, 10682–10692 (2012).
53. Sykora, R. E., Assefa, Z., Haire, R. G. & Albrecht-Schmitt, T. E. Hydrothermal synthesis, structure, Raman spectroscopy, and self-irradiation studies of $^{248}Cm(IO_3)_3$. *J. Solid State Chem.* **177**, 4413–4419 (2004).
54. Shannon, R. D. Revised effective ionic radii and systematic studies of interatomic distances in halides and chaleogenides. *Acta Crystallogr. A* **32**, 751–767 (1976).
55. Burns, J. H. & Baybarz, R. D. Crystal structure of americium sulfate octahydrate. *Inorg. Chem.* **11**, 2233–2237 (1972).
56. Cross, J. N. et al. Syntheses, structures, and spectroscopic properties of plutonium and americium phosphites and the redetermination of the ionic radii of Pu(III) and Am(III). *Inorg. Chem.* **51**, 8419–8424 (2012).

Methods

Caution!. ^{243}Am, ^{248}Cm, ^{247}Cm and ^{246}Cm, as well as their decay products, constitute serious health hazards because of their radioactive and chemical properties. All experiments involving radionuclides were conducted at the Lawrence Livermore National Laboratory in facilities designed for the safe handling of long- and short-lived radioactive materials and associated waste.

Materials. Americium samples were prepared by dilution of a primary standardized stock of ^{243}Am(III) chloride purchased from Eckert & Ziegler. Curium samples (97% ^{248}Cm + 3% ^{246}Cm + 0.01% ^{247}Cm) were prepared from a primary source purchased from Oak Ridge National Laboratory. CH_3COONa (≥99.9%), caesium chloride (>99.99%), $Na_2WO_4 \cdot 2H_2O$ (≥99%), boric acid, phosphoric acid and lanthanide trichloride salts (>99.9%) were purchased from chemical providers (VWR and MilliporeSigma) and used as received. All solutions were prepared using deionized water purified by the reverse osmosis cartridge system (≥18.2 MΩ cm). All experiments were performed in a temperature-controlled room (22 °C).

Synthesis of POMs. The following POM salts were synthesized according to literature procedures[57,58]. All the POM precursors used in the lanthanide–POM and actinide–POM syntheses were identified by powder XRD, Fourier transform infrared spectroscopy and Raman microscopy. $Na_9PW_9O_{39} \cdot 7H_2O$ was prepared by dissolving 12 g $Na_2WO_4 \cdot 2H_2O$ in 15 ml H_2O. Then, 0.4 ml of 85% H_3PO_4 was added dropwise. Afterwards, the pH was adjusted to 7–7.5 with glacial acetic acid (2.25 ml). During the addition, a solid immediately formed. The solid–solution slurry was stirred for 1 h, after which the solid was filtered under vacuum. PW_9 is unstable in solution at pH 7.5 and was converted into PW_{11} on binding to the trivalent lanthanide or actinide ions. $HK_8BW_{11}O_{39} \cdot 13H_2O$ was prepared by dissolving 30 g $Na_2WO_4 \cdot 2H_2O$ and 2 g H_3BO_3 in 50 ml boiling water. Afterwards, and while still boiling, 19 ml of 6 M HCl was added (to adjust to pH 6) under vigorous stirring. The solution was then boiled for an additional hour and then left to cool to room temperature. The solution was then placed at 4 °C for 24 h. Any solid that had formed after 24 h was removed by filtration and 10 g KCl was added to the solution. BW_{11} precipitated out of the solution as $HK_8BW_{11}O_{39} \cdot 13H_2O$. The solids were filtered under vacuum, dried and then redissolved (with a minimal amount of water) to recrystallize. The resulting crystals were used in the subsequent experiments with metal ions (actinides and lanthanides). $K_{10}P_2W_{17}O_{61} \cdot 20H_2O$ was prepared by first isolating the $K_6P_2W_{18}O_{62}$ precursor. Thus, 8 g of the P_2W_{18} salt, prepared by the method of Contant et al.[57], was dissolved in 20 ml water. To the P_2W_{18} aqueous solution, 2 g $HKCO_3$ was added and the mixture stirred for 1 h. Then, 10 g KCl was added to precipitate P_2W_{17}. The solid was filtered and dried under vacuum.

Synthesis of $M(W_5)_2$, $M(PW_{11})_2$, $M(BW_{11})_2$ and $M(P_2W_{17})_2$. Lanthanide or actinide chloride salts ($^{248}Cm^{3+}$ and $^{243}Am^{3+}$ from a parent stock solution in HCl) were dissolved in 0.1 M acetate buffer at pH 5.5, followed by the 1:2 stoichiometric addition of POMs to the cation (lanthanide concentrations were 100–1,000 µM, actinide concentrations were 10–20 µM). For spectroscopic measurements, the sample volume was 400–500 µl. For crystallization, 1:2 stoichiometric solutions of actinide–POM, containing 1–10 µg ^{248}Cm (or ^{243}Am), were prepared in 50–100 mM acetate buffer (100–1,000 µl, pH 5.5). Then, at room temperature, an aqueous solution of 6 M CsCl (or RbCl in the case of $Cm(W_5)_2$) was added gradually until the sample became transiently cloudy. The samples were then diluted with a minimal amount of H_2O (~100 µl) to bring the Cs–actinide–POM complexes slightly below their solubility limit. The samples were then left at room temperature. After 1–5 days under ambient conditions, several single crystals, with luminescence characteristic of Cm^{3+}, were visible to the naked eye (Fig. 1). Crystals of $Am(PW_{11})_2$ appeared yellow-red under ambient light (Supplementary Fig. 21). When the crystals were not deemed to be of XRD quality, they were redissolved with H_2O and the crystallization process restarted (Supplementary Figs. 3 and 4).

Single-crystal X-ray diffraction. Details of the crystallographic measurements and structures are given in Supplementary Figs. 24–27 and Supplementary Tables 6–13.

Fluorescence spectroscopy. Steady-state and time-resolved fluorescence spectra were measured with a FLS1000 spectrometer (Edinburgh Instruments) equipped with a double monochromator on the excitation and emission arms. A 450 W xenon lamp was used as light source for the steady-state measurements and a 60 W microsecond flashlamp was used for lifetime measurements (multichannel scaling single photon counting mode). Each lifetime decay curve contained 2,000 data points, with the maximum count per channel set to at least 1,000. The timespan of the acquisition was set so that the signal was measured until its return to background level. Fluorescence data for liquid samples were measured in sealed quartz cuvettes and the emission was collected at 90° relative to the excitation. Fluorescence spectra for solid samples were measured at 45° relative to the sample. Lifetimes were fitted using the Fluoracle computer program (Edinburgh Instruments). Quantum yields were measured using a 120 mm integrating sphere (Edinburgh Instruments).

UV-visible-NIR spectrophotometric titrations. Absorbance spectra of the ^{243}Am(III), ^{248}Cm(III), Nd(III) and Er(III) samples were measured using a high-performance Cary 6000i UV-visible-NIR spectrophotometer (Agilent Technologies). Samples were contained in sealed quartz cuvettes with a path length of 10 mm. The instrument was operated with narrow slits. Spectra were blank-corrected for buffer absorbance.

Raman microscopy. Raman spectra were collected using a Senterra II confocal Raman microscope (Bruker) equipped with high-resolution gratings (1,200 lines mm^{-1}), a 532 nm laser source (operated at 15 mW) and a thermoelectrically-cooled charge-coupled detector. The reported spectra are the average of at least five different spots per sample, each spot analysis consisting of 16 scans. The integration time was set to 400 ms per scan. No damage to the sample was observed due to laser irradiation.

^{31}P NMR spectroscopy. NMR experiments were conducted on a Bruker 600 MHz Avance III NMR spectrometer using a 14.10 T Bruker Ultrashield cryomagnet. The ^{31}P NMR spectra were recorded at an operating frequency of 242.938 MHz at 25 °C. Samples were loaded into 5 mm NMR tubes equipped with polytetrafluoroethylene liners for radioactive sample containment. Spectra were externally referenced to an 85% phosphoric acid solution in a mixture of 90% H_2O and 10% D_2O at 0 ppm. Before the collection of data, a ^{31}P 90° pulse width was calibrated on either the sample or phosphoric acid reference. The recycle delay was set to three to five times the T_1 value for each sample to ensure equal excitation of all peaks. The number of scans collected for the Eu–PW_{11} sample was 256 and 1,024 for Am–PW_{11}.

Synthesis of $M(POM)_2$ for solution characterization. $M(POM)_2$ were synthesized by dissolving the corresponding metal chloride salt in 0.1 M acetate buffer at pH 5.5, or by diluting an aliquot of the parent stock solution (for example, $AmCl_3$ or $CmCl_3$ stock solution in 0.1 M HCl) in the desired buffer. For the lanthanide salts, the final sample concentration ranged from 100 to 1,000 µM, and for the actinides, the concentration ranged from 10 to 20 µM. A stoichiometric amount of POM stock solution (in the same buffer) was added to the metal solution to obtain a metal/POM ratio of 1:2. For $M(W_5)_2$, instead of synthesizing the corresponding POM, it was prepared in situ by dissolving Na_2WO_4 following a similar procedure to that described above. Spectroscopic measurements were performed in quartz cuvettes using a sample volume of 400 µl, corresponding to 1–2 µg actinide. Given the observed signal intensity of the Cm–POM solutions, we estimated that the amount of material in the samples could be further decreased by a factor of ~100.

Synthesis of $M(POM)_2$ for SCXRD and Raman microscopy. $M(POM)_2$ were synthesized using a similar method to that described above. However, for crystallization, an ~100 µl aliquot was taken from an ~500 µM $Cm(POM)_2$ or $Am(POM)_2$ solution. A 6 M CsCl solution was titrated into the aliquot, to the point of incipient precipitation. A small amount of H_2O (~100 µl) was then added to obtain a clear sample. At this point, the solution, with a controlled opening, was left for 1–5 days, during which time single crystals of $Cm(POM)_2$ or $Am(POM)_2$ grew. After a few days under ambient conditions, several single crystals (with characteristic luminescence in the case of Cm^{3+}) were visible to the naked eye. If the crystal quality was not satisfactory, the crystals were redissolved using a different volume of H_2O and the crystallization process restarted. In these syntheses, 6 µg ^{248}Cm was used to obtain the $Cm(BW_{11})_2$ crystals, 12 µg ^{248}Cm to obtain both isomers of $Cm(PW_{11})_2$, and 5 µg ^{243}Am for each of $Am(BW_{11})_2$ and $Am(PW_{11})_2$-α. This procedure is a one-pot, room-temperature, all-aqueous synthesis, so no loss of material occurred during the syntheses.

Data availability

All data that support the conclusions in this study are present in the manuscript and/or the Supplementary Information. Crystallographic data for the structures reported in this Article have been deposited at the Cambridge Crystallographic Data Centre under the following CCDC accession codes: 2105534 ($CmPW_{11}$-α), 2105535 ($CmPW_{11}$-β), 2105623 ($NdPW_{11}$), 2105638 ($EuPW_{11}$), 2114774 ($CmBW_{11}$), 2114775 ($EuBW_{11}$), 2127430 ($NdBW_{11}$), 2127431 ($SmBW_{11}$), 2127432 ($SmPW_{11}$), 2127433 (EuW_5) and 2127434 (NdW_5). Copies of the data can be obtained free of charge via https://www.ccdc.cam.ac.uk/structures/. Source data are provided with this paper.

References

57. Contant, R., Klemperer, W. G. & Yaghi, O. in *Inorganic Syntheses* Vol. 27 (ed. Ginsberg, A. P.) 104–111 (Wiley, 1990).
58. Tézé, A., Michelon, M. & Hervé, G. Syntheses and structures of the tungstoborate anions. *Inorg. Chem.* **36**, 505–509 (1997).

Acknowledgements

This work was performed under the auspices of the US Department of Energy (DOE) by the Lawrence Livermore National Laboratory under contract DE-AC52-07NA27344 and was supported by the LDRD Program under the LLNL project 20-LW-017. Release number: LLNL-JRNL-829648. I.C. and M.N. acknowledge the US DOE, National Nuclear Security Administration (NNSA) for work conducted at Oregon State University, award number DE-NA0003763. I.C. acknowledges the US DOE's SCGSR fellowship.

Author contributions

G.J.-P.D. supervised the project. I.C. and G.J.-P.D. conducted the synthetic and spectroscopic experiments. I.C., J.R.I.L., M.N. and G.J.-P.D. conducted the crystallography experiments and analysed the crystallographic data. C.A.C., H.E.M. and A.M.S. conducted the NMR experiments. G.J.-P.D. wrote the original draft of the manuscript. G.J.-P.D., M.N. and M.Z. acquired funding. All authors made intellectual contributions to the project, and also reviewed and edited the manuscript.

Competing interests

The authors declare no competing interests.

Additional information

Supplementary information The online version contains supplementary material available at https://doi.org/10.1038/s41557-022-01018-8.

Correspondence and requests for materials should be addressed to Gauthier J.-P. Deblonde.

Peer review information *Nature Chemistry* thanks Kristina Kvashnina, Annette Rompel and the other, anonymous, reviewer(s) for their contribution to the peer review of this work.

Reprints and permissions information is available at www.nature.com/reprints.